Since January 2020 Elsevier has created a COVID-19 resource centre with free information in English and Mandarin on the novel coronavirus COVID-19. The COVID-19 resource centre is hosted on Elsevier Connect, the company's public news and information website.

International Journal for Parasitology 41 (2011) 81–88

Contents lists available at ScienceDirect

International Journal for Parasitology

journal homepage: www.elsevier.com/locate/ijpara

Reduced activity of the epithelial sodium channel in malaria-induced pulmonary oedema in mice

Leia Hee [a], Anuwat Dinudom [b], Andrew J. Mitchell [a], Georges E. Grau [a], David I. Cook [b], Nicholas H. Hunt [a], Helen J. Ball [a,*]

[a] Discipline of Pathology, School of Medical Sciences and Bosch Institute, University of Sydney, NSW 2006, Australia
[b] Discipline of Physiology, School of Medical Sciences and Bosch Institute, University of Sydney, NSW 2006, Australia

ARTICLE INFO

Article history:
Received 2 July 2010
Received in revised form 22 July 2010
Accepted 23 July 2010

Keywords:
Malaria
Lung
Pulmonary oedema
ENaC
Sodium transport
Mouse model

ABSTRACT

Lung complications during malaria infection can range from coughs and impairments in gas transfer to the development of acute respiratory distress syndrome (ARDS). Infecting C57BL/6 mice with *Plasmodium berghei* K173 strain (PbK) resulted in pulmonary oedema, capillaries congested with leukocytes and infected red blood cells (iRBCs), and leukocyte infiltration into the lungs. This new model of malaria-associated lung pathology, without any accompanying cerebral complications, allows the investigation of mechanisms leading to the lung disease. The activity of the amiloride-sensitive epithelial sodium channel (ENaC) in alveolar epithelial cells is decreased by several respiratory tract pathogens and this is suggested to contribute to pulmonary oedema. We show that PbK, a pathogen that remains in the circulation, also decreased the activity and expression of ENaC, suggesting that infectious agents can have indirect effects on ENaC activity in lung epithelial cells. The reduced ENaC activity may contribute to the pulmonary oedema induced by PbK malaria.

1. Introduction

Each year there are estimated to be several hundred million malaria infections. Most of these are uncomplicated, but the complications that comprise severe malaria have a high mortality rate. Manifestations of severe malaria include cerebral malaria, severe anaemia and malaria-associated acute respiratory distress syndrome (ARDS). Most cases of severe malaria are caused by *Plasmodium falciparum* infection, although ARDS occasionally occurs during *Plasmodium vivax* infection (reviewed in Tan et al., 2008). Cerebral malaria, malaria-associated ARDS and severe anaemia can occur simultaneously, but many patients do not develop all three of the complications or may manifest them at different times during infection. ARDS may occur at the time of presentation (Charoenpan et al., 1990) or after the commencement of treatment when the parasitaemia is falling (Brooks et al., 1968).

An autopsy series on patients with malaria-associated ARDS revealed pulmonary oedema, congested pulmonary capillaries, thickened alveolar septa, hyaline-membrane formation and intra-alveolar haemorrhage (Brooks et al., 1968). Studies of non-immune adults with severe malaria found that 21–23% of cases developed pulmonary oedema (Lichtman et al., 1990; Aursudkij et al., 1998). Although respiratory distress is common amongst children with severe malaria, it is often associated with metabolic acidosis rather than pulmonary oedema.

ARDS is at the most severe end of the spectrum of lung manifestations of malaria and, fortunately, occurs infrequently. Milder respiratory signs are observed with a much higher frequency in uncomplicated falciparum, vivax and ovale malaria (Anstey et al., 2002). These signs include coughing, impairments in gas transfer and increased pulmonary phagocytic activity. Treatment of vivax malaria infection resulted in greater pulmonary phagocytic activity and the deterioration of gas transfer at the alveolar-capillary membrane, suggesting an increased inflammatory response (Anstey et al., 2002, 2007). A review of acute lung injury and ARDS in *P. vivax* infection noted that the complications occurred after commencement of treatment and generally did not involve other organs (Tan et al., 2008).

At present little is understood about the mechanisms that lead to the development of lung complications in malaria. Animal models provide a useful tool for studying pathogenesis and the experimental cerebral malaria (ECM) model of *Plasmodium berghei* ANKA strain (PbA) infection has been used for many years to provide insights into human cerebral malaria (reviewed in de Souza et al., 2010). Infection of susceptible mouse strains with PbA results in pulmonary oedema (Senaldi et al., 1994; Chang et al., 2001; Schofield et al., 2002; Lovegrove et al., 2008), but the development

* Corresponding author. Address: Molecular Immunopathology Unit, Discipline of Pathology, Medical Foundation Building, University of Sydney, Camperdown, NSW 2006, Australia. Tel.: +61 2 9036 3238; fax: +61 2 9036 3286.
E-mail address: helen.ball@sydney.edu.au (H.J. Ball).

0020-7519/$36.00 © 2010 Published by Elsevier Ltd. on behalf of Australian Society for Parasitology Inc.
doi:10.1016/j.ijpara.2010.07.013

and rapid progression of cerebral malaria in these mice makes it difficult to study mechanisms leading to lung complications. This has been circumvented by using an inbred strain of mice, DBA/2, which is resistant to ECM but susceptible to lung complications (Epiphanio et al., 2010). In addition, infection of C57BL/6 mice with *P. berghei* NK65 strain produced pathology resembling malaria-associated ARDS in humans but without any cerebral symptoms (Van den Steen et al., 2010). In this study we describe a model of malaria-associated lung pathology with a comparatively mild disease phenotype. Mice infected with *P. berghei* K173 strain (PbK) develop pulmonary oedema associated with an inflammatory interstitial infiltrate, in the absence of signs of cerebral malaria. Mechanistically, we demonstrate that the activity of amiloride-sensitive epithelial sodium channels (ENaC) decreases during infection and this may contribute to the development of oedema.

2. Materials and methods

2.1. Animals

Seven to 8 week old female mice were used in all studies. C57BL/6 mice were obtained from the Australian Animal Research Centre (Perth, Australia). All in vivo manipulations were performed and monitored in accordance with the guidelines established by the University of Sydney (Australia) Animal Ethics Committee.

2.2. Parasite inoculation and PbK-induced murine malaria

Plasmodium berghei K173 strain (PbK) was obtained from Dr. Ian Clark of the Australian National University in Canberra, Australia. Mice were inoculated i.p. with 2×10^6 infected red blood cells (iRBCs) from a PbK-infected mouse. Progression of malaria was monitored by determining parasitemia and haematocrit levels from blood taken in a tail prick of infected mice. Parasite levels were monitored during the course of the infection by methanol-fixed blood smears stained with the Diff-Quick stain set (IMEB).

2.3. Phenylhydrazine (PHZ) treatment

Mice were injected i.p. with 60 mg/kg PHZ (Sigma) on days 0 and 1. A half dose of PHZ was given on day 3. Haematocrit was monitored daily from tail-vein blood to observe that it was lower than 20% for 4 days, so as to mimic the degree of anaemia in PbK malaria infection.

2.4. Pulmonary oedema and bronchoalveolar lavage (BAL) evaluation

The unperfused lung was weighed after removal, dried for 2 days in an oven at 50 °C and re-weighed. From the wet weight and dry weight, changes in lung water and solid content in PbK infection were calculated. To collect BAL fluid, mice were anesthetized with an isofluorane mask. The trachea was exposed and a 22-gauge needle inserted into the lumen of the trachea. The connected syringe was used to gently lavage each mouse three times with 1 ml of PBS. The washes were pooled and the protein concentration measured using a Bicinchoninic acid protein assay (Pierce).

2.5. Lung histology and immunohistochemistry

Lungs were fixed for histology with 10% (w/v) formalin. After fixation, the lungs were embedded in paraffin, cut into 7 μm sections, and stained with H&E. For immunohistochemistry, sections were deparaffinized and rehydrated. Endogenous peroxidase was blocked for 20 min by incubating with 0.3% hydrogen peroxide in methanol. Antigen retrieval was performed at 100 °C in 0.01 M citrate buffer, pH 6.0 for 10 min. For the ENaCβ subunit immunostaining there was an additional blocking step for 10 min with avidin and 10 min with biotin using a Biotin Blocking kit (DAKO, Denmark). After washing, sections were blocked for 30 min with TNB blocking buffer (0.1 M Tris–HCl buffer, pH 7.5, 0.15 M NaCl and 0.5% (w/v) blocking reagent (PerkinElmer, USA)). All washes were performed three times for 5 min in TNT buffer (0.1 M Tris–HCl buffer, pH 7.5 containing 0.3 M NaCl and 0.05% (v/v) Tween 20). Rabbit anti-human fibrinogen antibody (DAKO) was used for the detection of fibrinogen in the mouse lung at a dilution of 1:2500 in TNB blocking buffer for 30 min. Rabbit anti-ENaC antibody (courtesy of S. Townley, Institute of Medical and Veterinary Science, South Australia) was used for the detection of β-ENaC in the mouse lung at a dilution of 1:5000 in TNB blocking buffer for 30 min. After washing, secondary detection used a biotinylated anti-rabbit antibody with the EnVision detection system (DAKO). Staining was visualised by incubating the sections in 3,3′-diaminobenzidine and then counterstaining the sections with haematoxylin. The sections were then dehydrated and coverslipped. Isotype controls (rabbit IgG) and method controls (no primary antibody) were included.

2.6. Quantification of β-ENaC expression

Sections from lungs of five uninfected and five infected mice were immunostained in one run with the same incubation times and solutions. Sections were coded so that the investigator was unaware of their infection status and images of bronchioles were captured using an Olympus IX71 microscope. Every visible bronchiole in the section (6–12 bronchioles/section) was selected, apart from some on the very edge of the sections where the staining did not appear to be specific. The AnalySIS Five program (Olympus) was used to designate an area around the epithelial cells of the bronchiole. A second area was defined within the lumen. The signal corresponding to the wavelength of the brown staining was measured and converted into a grey scale. The intensity of these signals was used to calculate the pixels in each square micron. The intensity of the second defined area was subtracted from the first area to determine the expression within the cells. The values obtained from each bronchiole were averaged over the section.

2.7. Preparation of single cell suspension from lung homogenates

Anaesthetized animals were perfused with 10 ml PBS containing 20 U/ml heparin through the right ventricle. The heart and lungs were removed en bloc and the heart, thymus and lymph nodes were dissected away. The lungs were minced and placed in PBS containing 5% (v/v) FBS, 1 mg/ml collagenase (Sigma), and DNase (Boehringer Mannheim) for 60 min at 37 °C on a gentle shaking platform. Lungs were further disrupted by aspiration through an 18-gauge needle and then pushed gently through a cell strainer. The cell suspension was centrifuged at 350*g* for 10 min at 4 °C. The pellet was resuspended in 10 ml Percoll (20%, w/v) and centrifuged at 500*g* for 15 min at 4 °C. The upper Percoll layer containing debris and clumps was removed and the remaining cell pellet washed twice with PBS containing 5% FBS. RBCs within the lung homogenates were lysed using 1 ml distilled water for 1 min. Total cell numbers per lung were determined using a hemocytometer.

2.8. Flow cytometric analysis of cell surface markers

Flow cytometry staining on Fc-blocked (pre-incubated with unlabelled anti-CD16/32, clone 2.462) lung cells was performed by standard methods using the following antibodies: anti-CD4 (clone RM4-5), anti-CD8 (clone 53-6.7), anti-CD3 (clone 145-2C11), anti-CD11c (clone HL3), anti-CD11b (Mac-1, clone M1/70) and anti-CD45 (clone 30-F11). Antibodies were sourced from Bec-

ton Dickinson and eBioscience as direct conjugates to FITC, phycoerythrin (PE), PECy5 or PECy7. Data were acquired using a FC500 (Beckman Coulter) and analysed using Flowjo software, version 8.8.6 (Tree Star, USA). Lung myeloid populations were identified based on autofluorescence (AF) patterns and surface staining for Ly6G, CD11b and CD11c (Vermaelen and Pauwels, 2004; Mitchell et al., 2010). Fluorescence-minus one (FMO) controls (Perfetto et al., 2004) were used to assess background staining.

2.9. ENaC subunit mRNA expression

A mouse lung was homogenised in 1 ml of Tri reagent (Sigma) and RNA was purified according to the manufacturer's protocol. Contaminating genomic DNA was removed using a DNAfree kit (Ambion). Reverse transcription was performed using 4 μg total RNA, 0.1 μg oligo $(dT)_{18}$, 5 U RNaseOUT (Invitrogen) and a Moloney murine leukaemia reverse transcriptase kit (Invitrogen). Real time quantitative (qRT-)PCR was performed using 20 ng cDNA, 100 nM of each primer and Platinum SYBR green qPCR SuperMix-UDG (Invitrogen) in a Rotor-Gene 3000 (Corbett Research, Australia). An 8 min denaturation at 95 °C was followed by 40 cycles of 15 s at 95 °C and 45 s at 60 °C. The identity and purity of PCR products were assessed by melting curve analysis. Expression was normalised to the reference gene ribosomal protein L13a (RPL13a). Relative expression of the ENaC subunits was calculated using the ΔΔCT method after determining the primer sets had similar amplification efficiencies.

ENaCα: 5′-CACCTTTGCTTTTGTGAACTCG-3′, 5′-CATCCCTGAGCACAGTTCAGTC-3′
ENaCβ: 5′-CACCTCAGTCTCCCAGAATCCT-3′, 5′-CGTGTTCCCCTTTCAAGACTTC-3′
ENaCγ: 5′-TGGTATGCTGCGAGCTGTACTA-3′, 5′-GTAGGCTGGTGTTTGTTATGCG-3′
RPL13a: 5′-CTTAGGCACTGCTCCTGTGGAT-3′, 5′-GGTGCGCTGTCAGCTCTCTAAT-3′

2.10. ENaC activity

Freshly collected tracheae were transferred to a modified Ussing Chamber. Apical and basolateral surfaces of trachea were simultaneously perfused with a solution containing 130 mM NaCl, 1 mM $CaCl_2$, 1 mM KCl, 1 mM $MgCl_2$, 5 mM glucose, 10 mM HEPES, pH 7.4, maintained at 37 °C. Experiments were carried out under open-circuit conditions (Kunzelmann et al., 2000). Transepithelial resistance was measured by applying short (1 s) repetitive 10 μA current pulses across the epithelium. The transepithelial potential differences (V_{te}) were measured with reference to the luminal side of the epithelium, and equivalent short-circuit current was calculated according to Ohm's law. Amiloride-sensitive equivalent short-circuit current (I_{ami}) was determined as the change in current ($I_{ami(relative)}$).

2.11. Statistical analysis of data

Data from all experiments were analysed for statistical significance using GraphPad Prism 5.0. Comparisons of two groups used a two-tailed *t*-test. One-way ANOVA was used for comparisons of more than two groups followed by a Tukey's multiple comparison post-test. Data were expressed as the mean ± S.E.M. and statistical significance was reached at $P < 0.05$.

3. Results

3.1. Progression of PbK infection

Mice were infected i.p. with 2×10^6 iRBCs and sacrificed on days 3, 6, 9, 12 or 15 p.i. for analysis of their lung pathology. PbK infection with this number of iRBCs has previously been shown by our laboratory not to cause cerebral malaria (Mitchell et al., 2005). The lungs of the infected mice were significantly heavier from day 9 onwards (Fig. 1A). This was partially due to the accumulation of proteins

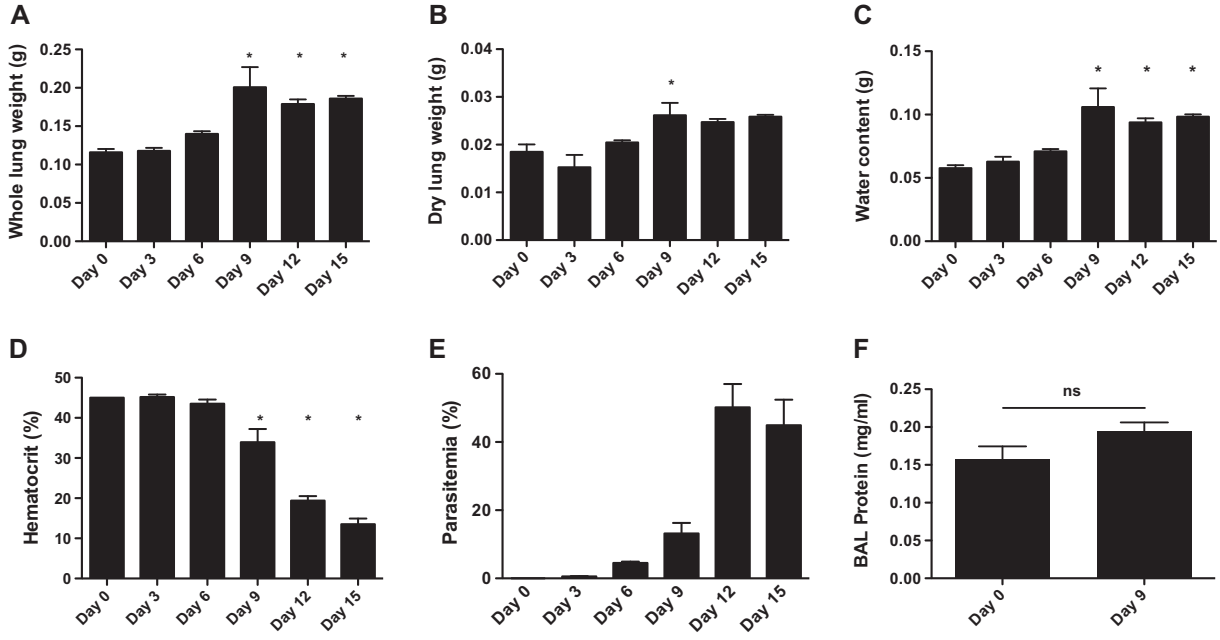

Fig. 1. Progression of *Plasmodium berghei* K173 strain (PbK) infection in the lung. PbK-infected mice were sacrificed on days 0, 3, 6, 9, 12 and 15 p.i., then the whole unperfused lungs were weighed (A). One lung was dried and re-weighed to determine the dry weight (B). The difference in weight was used to calculate the water content of the tissue (C). At the time of death the haematocrit (D) and parasitaemia (E) of the mice were recorded. In a separate experiment, bronchoalveolar lavage (BAL) fluid was collected from euthanased uninfected and PbK-infected mice (day 9 p.i.) for measurement of protein concentration (F). Data represent mean ± S.E.M., $n = 6$. *Denotes significant difference ($P < 0.05$). ^{ns}Denotes not statistically significant ($P < 0.05$).

and cells in the tissue, as the dry weight of the lungs also increased (Fig. 1B). The water content of the lung also increased during infection, indicating the development of oedema (Fig. 1C). The parasitaemia reached over 60% by day 12 (Fig. 1E) and the haematocrit declined to approximately 50% of its baseline level (Fig. 1D). The protein concentration of the BAL fluid was not significantly different in the PbK-infected mice (Fig. 1F), suggesting that the oedematous fluid was not proteinaceous.

A histopathological analysis showed extensive leukocyte infiltration into the interstitium, thickened alveolar septa and congested pulmonary capillaries (Fig. 2A and B). Immunohistochemistry to detect a plasma protein, fibrinogen, indicated that the pulmonary endothelium was permeabilized in the infected mice, allowing plasma proteins to leak into the interstitium (Fig. 2C–F). However, in concordance with the protein measurements of the BAL fluid, the alveoli appeared clear of fibrinogen staining.

3.2. Leukocyte populations in PbK-infected lungs

The cellular infiltrate seen in the lungs of PbK-infected animals consisted of a mix of inflammatory myeloid cells and T cell subsets. Neutrophils (AF^{low}, $Ly6G^{high}$ cells) increased in number in the lungs of mice as the infection progressed, with approximately 30-fold more neutrophils being found in the lung at day 12 p.i. compared with uninfected mice (Fig. 3A). Monocytes ($AF^{int/lo}$, $Ly6G^{neg}$, $CD11b^{hi}$, $CD11c^{neg/lo}$) were also prominent in the infiltrate. The numbers of these cells increased approximately 35-fold over the course of infection, to reach levels similar to those of neutrophils (Fig. 3B). In contrast to the striking changes in inflammatory cells, the numbers of pulmonary dendritic cells ($AF^{int/lo}$, $Ly6G^{neg}$, $CD11b^{neg}$, $CD11c^{hi}$) increased modestly during infection (approximately threefold – Fig. 3C), while resident alveolar macrophages (AF^{hi}, $Ly6G^{neg}$, $CD11b^{neg}$, $CD11c^{hi}$) remained unchanged over the course of the infection (Fig. 3D). T cell subsets were also a feature of the cellular infiltrate. Numbers of $CD4^+$ T cells ($CD45^{pos}$, $CD3^{pos}$, $CD4^{pos}$) progressively increased in the lung during malaria infection and were over 20-fold higher at day 12 p.i. compared with uninfected mice (Fig. 3E). Changes in $CD8^+$ T cell numbers ($CD45^{pos}$, $CD3^{pos}$, $CD8^{pos}$) were even more dramatic. These cells significantly increased in number by day 6 and peaked at over 110-fold higher in the PbK-infected mice at day 12 p.i. compared with uninfected mice (Fig. 3F).

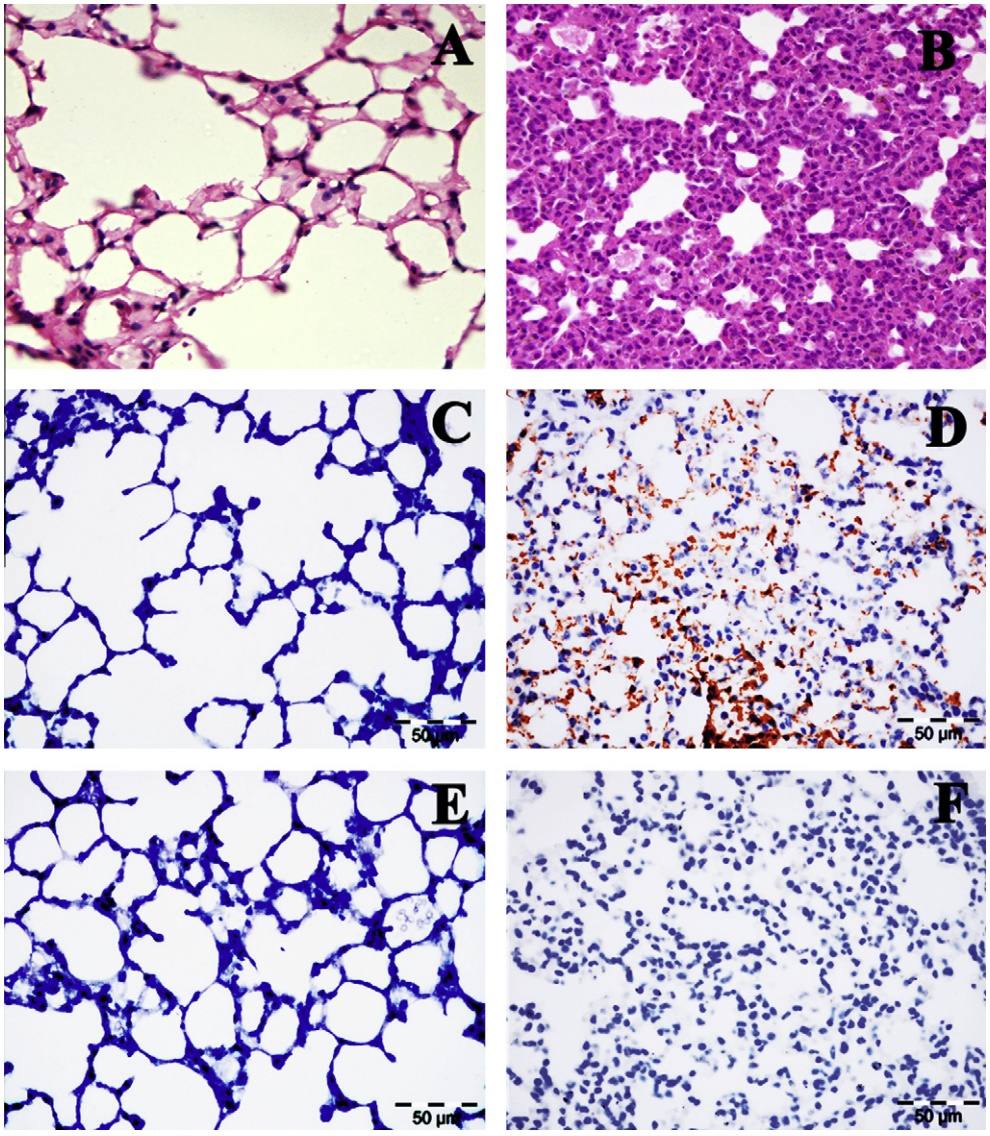

Fig. 2. *Plasmodium berghei* K173 strain (PbK)-associated lung pathology. Representative images of lung sections stained with H&E from uninfected (A) and PbK-infected (day 9 p.i.) (B) mice. The tissues were also immunostained with an antibody for fibrinogen. (C) and (E) Control mice. (D) and (F) Infected mice. (C) and (D) Show staining with an anti-fibrinogen primary antibody whilst the sections shown in (E) and (F) were stained with an isotype control.

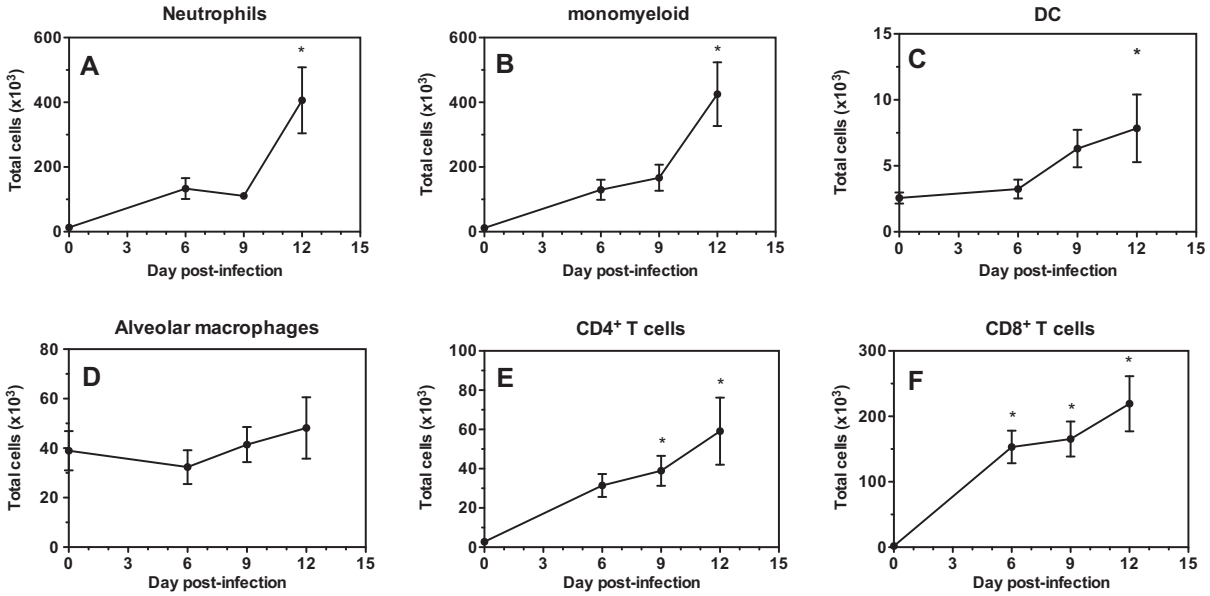

Fig. 3. Cell sub-populations in the lung. *Plasmodium berghei* K173 strain (PbK)-infected mice were sacrificed on days 0, 6, 9 and 12 p.i. A cell suspension was prepared from the perfused lungs and flow cytometry was used to identify cell sub-populations. (A) Neutrophils were identified as autofluorescence (AF)low, Ly6G^{high} cells. (B) Monocytes were identified as AF$^{int/lo}$, Ly6G^{neg}, CD11b^{hi}, CD11c$^{neg/lo}$ cells. (C) Pulmonary dendritic cells (DC) were identified as AF$^{int/lo}$, Ly6G^{neg}, CD11b^{neg}, CD11c^{hi} cells. (D) Resident alveolar macrophages were identified as AF^{hi}, Ly6G^{neg}, CD11b^{neg}, CD11c^{hi} cells. (E) CD4$^+$ T cells were identified as CD45^{pos}, CD3^{pos}, CD4^{pos} cells. (F) CD8$^+$ T cell numbers were identified as CD45^{pos}, CD3^{pos}, CD8^{pos} cells. Data represent mean ± S.E.M., $n = 6$. *Denotes significant difference ($P < 0.05$).

3.3. ENaC expression and activity in PbK-infected lungs

Sodium in the alveolar fluid enters the apical membranes of alveolar type II cells mainly through the amiloride-sensitive ENaC and is actively transported across the basolateral membranes of these cells into the blood by the Na/K-ATPase. Alveolar fluid is reabsorbed across the epithelium by the resulting osmotic gradient generated by Na^+ absorption (Matalon et al., 1991). ENaC is formed from three subunit proteins, α-, β- and γ-ENaC, and levels of ENaC expression have been found to correlate with Na^+ and fluid reabsorption in the lung (Li and Folkesson, 2006). Expression of the ENaC subunits in the lung was measured by qRT-PCR. We found that PbK infection did not significantly alter expression of the ENaC subunit mRNAs (Table 1). We used quantitative immunohistochemistry to measure expression of the β subunit protein of ENaC in the epithelium of the bronchioles (Fig. 4A and B). Expression of β-ENaC was significantly decreased in the lung epithelia of PbK-infected mice at day 10 p.i. to approximately two-thirds of the level observed in uninfected mice (Fig. 4C). To investigate an effect of PbK infection on Na^+ transport in the respiratory epithelium, we determined the amiloride-sensitive current, which represents activity of ENaC, in isolated mouse trachea. Tracheas dissected from uninfected and infected mice were mounted in a modified Ussing chamber and the equivalent short-circuit current was measured under open-circuit conditions. We found that the amiloride-sensitive equivalent short-circuit current of the trachea of PbK-infected mice, 5.3 ± 3.3 μA/cm^2, was significantly lower that that of the uninfected mice, 16.9 ± 3.6 μA/cm^2 (Fig. 4D).

Table 1
Expression of epithelial sodium channel (ENaC) subunit mRNA in *Plasmodium berghei* K173 strain (PbK)-infected mice (day 9 p.i.).

ENaC subunit	Relative expression[a]
α	1.07 ± 0.63[b]
β	1.48 ± 0.33[b]
γ	0.87 ± 0.20[b]

[a] Relative to uninfected mice, mean ± S.E.M., $n = 9–12$.
[b] No significant difference compared with uninfected mice, $P < 0.05$.

3.4. Effect of PHZ-induced anaemia on lung oedema and ENaC activity

Rats exposed to hypoxic conditions have reduced ENaC activity (Vivona et al., 2001) and incubating alveolar type II cells under hypoxia decreases expression of the ENaC protein at the apical surface (Planes et al., 2002). PbK infection causes severe anaemia (Fig. 1D) that may result in tissues experiencing hypoxic conditions. Therefore, we investigated whether chemically inducing anaemia would affect ENaC activity and pulmonary oedema. PHZ was administered to uninfected mice to chemically induce the levels of anaemia observed during PbK infection (Fig. 5A). The PHZ-treated mice did not develop significant lung oedema (Fig. 5B) or loss of ENaC activity (Fig. 5C).

4. Discussion

We described a model of malaria-associated lung pathology caused by infection with PbK that resembles mild pulmonary pathology in humans. Following infection, mice progressively accumulated leukocytes, including neutrophils and CD8$^+$ T cells, in the interstitial spaces of their lungs and the alveolar septa became swollen. Fibrinogen leakage into the interstitium suggests increased permeability of the endothelium to plasma proteins. The fluid content of the lung also increased significantly as the mice developed pulmonary oedema. These features of PbK infection in mice are also found in humans with malaria-associated ARDS (Brooks et al., 1968) as well as mouse models of malaria-associated ARDS (Epiphanio et al., 2010; Van den Steen et al., 2010).

PbK infection resulted in large numbers of myeloid cells (monocytes and neutrophils) being recruited to the lungs and transmigrating across the endothelium. Mediators released by neutrophils, such as proteases and oxidants, have the potential to damage host cells as well as control infections. Mice deficient in

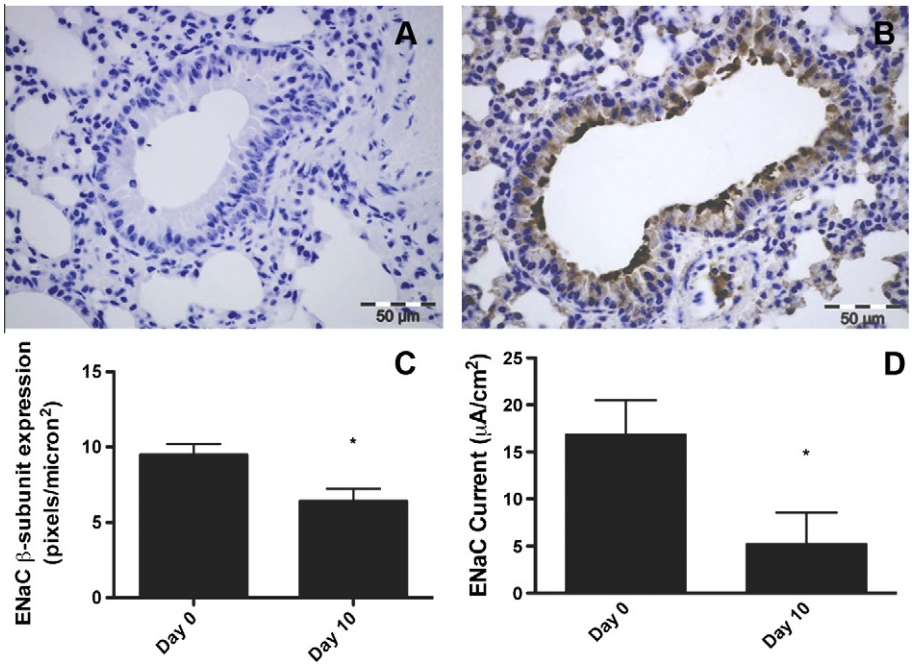

Fig. 4. Epithelial sodium channel (ENaC) activity and expression. Lung sections from uninfected and *Plasmodium berghei* K173 strain (PbK)-infected (day 10 p.i.) mice were immunostained with an antibody for the β-ENaC subunit. A representative image from an uninfected lung stained with the isotype control (A) or anti-β-ENaC antibody (B) is shown. β-ENaC expression was quantified as described in Section 2 and expressed as mean ± S.E.M., $n = 5$ (C). The amiloride-sensitive current due to ENaC activity was measured in tracheal preparations from uninfected and PbK-infected (day 10 p.i.) mice (D). Data are expressed as mean ± S.E.M., $n = 6$. *Denotes statistical significance ($P < 0.05$).

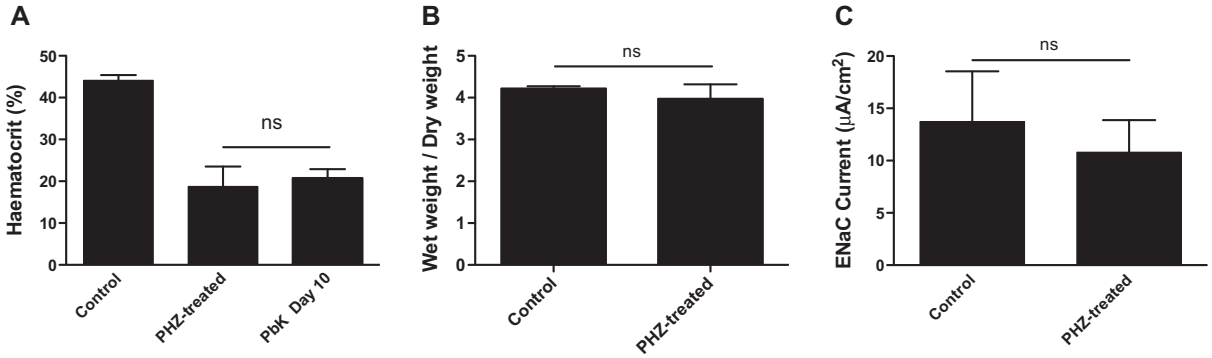

Fig. 5. Phenylhydrazine (PHZ)-induced anaemia and oedema. Mice treated with PHZ developed anaemia similar in degree to that in *Plasmodium berghei* K173 strain (PbK) infection (A). Oedema in the lungs was assessed by calculating the ratio of the weight of the wet lungs over the dry lungs (B). The amiloride-sensitive current due to epithelial sodium channel (ENaC) activity was measured in control and PHZ-treated mice (C). Data are expressed as mean ± S.E.M., $n = 7–9$. ^{ns}Denotes not statistically significant ($P < 0.05$).

chemoattractants for neutrophils have reduced lung injury and neutrophil sequestration in a non-malarial ARDS model (Belperio et al., 2002). Additional cell types sequestered in the lungs during PbK infection include $CD4^+$ and $CD8^+$ T cells. Cytotoxic $CD8^+$ T cells localise to the brain during PbA infection (Belnoue et al., 2002) and damage the brain endothelium in a perforin-dependent manner (Potter et al., 2006). These cells are also required for PbA-induced respiratory distress (Chang et al., 2001). Furthermore, in PbNK65 infection, treatment with dexamethasone decreases numbers of $CD8^+$ T cells, $CD4^+$ T cells and macrophages in the lung and prevents disease progression, as measured by changes in lung weight, suggesting that infiltrating cells may play a pathogenic role in malaria-associated lung pathology (Van den Steen et al., 2010).

Other features of ARDS include an exudate of proteinaceous fluid and leukocytes within the alveoli and hyaline-membrane formation. These signs are observed in autopsies of patients with malaria-associated lung pathology (Brooks et al., 1968) and in mouse models of malaria-associated ARDS (Epiphanio et al., 2010; Van den Steen et al., 2010). In contrast, damage or dysfunction of the alveolar epithelial layer during PbK infection appears minimal as the fluid in the alveoli does not significantly increase in protein content and the alveolar spaces are mostly free of leukocytes. In addition, there is no evidence of intra-alveolar haemorrhage and hyaline-membrane formation. During infection with PbNK65 the dry weight of the lung increases approximately 100% (Van den Steen et al., 2010) compared with approximately 30% in PbK infection. This difference is likely due to the proteinaceous fluid and cells infiltrating the alveolar spaces observed in the PbNK65 model. This suggests that whilst there is disruption or damage to the endothelium in the PbK model, there is little damage to the alveolar epithelium. Therefore, the model described here does not represent a model of malaria-associated ARDS but a milder form of lung injury, similar to that seen in many human malaria infections (Anstey et al., 2002, 2007).

The presence of circulating antigen and immune mediators suggests that the pathophysiology of malaria infection has parallels to sepsis (Clark and Cowden, 2003). One of the most common causes of acute lung injury and ARDS is sepsis and this is often modelled in rodents by administration of bacterial lipopolysaccharide (LPS). An ultrastructural study comparing lung pathology in mice inoculated with LPS either directly into their respiratory tract or into their circulation revealed different pathological features (Menezes et al., 2005). All of the LPS-treated mice showed increased tissue cellularity and collapse of the alveoli spaces; however, the mice with LPS instilled directly into their respiratory tract also showed greater infiltration of neutrophils into the alveoli and damage to the epithelial layer. Thus the PbK model of malaria-associated lung pathology has greater similarity to models where lung injury is induced by systemic injection of LPS to mimic sepsis. The pathogenesis of PbK-associated lung pathology likely begins with damage to the endothelium, by this sepsis-like process, allowing proteins to enter the interstitium. These could include malaria antigens, as well as plasma proteins. Subsequently leukocytes enter the interstitium in response to the abnormal presence of these proteins. An increase in interstitial pressure can lead to fluid being forced into the alveolar spaces.

In humans, ARDS is a severe but uncommon manifestation of malaria-associated lung pathology that has a high mortality rate. Rodent malaria-ARDS models may become valuable tools for investigating therapeutic agents for malaria-associated ARDS (Epiphanio et al., 2010; Van den Steen et al., 2010). However, much lung pathology associated with malaria infection is milder and comparatively common. These observations include coughing, chest crackles and impairments in gas transfer (Anstey et al., 2002, 2007). In *P. vivax* infection, gas transfer deteriorated and phagocytic activity increased after the initiation of anti-malaria treatment and this effect was postulated to be due to an increased inflammatory response to killed parasites (Anstey et al., 2002, 2007). PbK-infected lungs have capillaries congested with iRBCs and leukocytes and it is likely that killed parasites will release antigens that intensify the inflammatory response. Therefore, the PbK model could be a useful tool to investigate the interaction between anti-malarial treatments and lung complications.

There are evident changes in the fluid balance during PbK infection in the absence of damage to the epithelium. Alveolar type I and II cells express a number of ion channels. Of these, ENaC is unlikely to be the major regulator of alveolar fluid clearance under normal conditions (Li and Folkesson, 2006). Its activity has been shown to increase significantly in situations such as pulmonary oedema (Elias et al., 2007) and at birth (Li et al., 2007), a time when dramatic changes in alveolar lung fluid clearance occur. Regulation of ENaC activity is highly complex and can be modulated by mRNA and protein expression, proteolytic processing, ubiquitination and intracellular trafficking.

ENaC activity is decreased during infection with a variety of pathogens, including respiratory syncytial virus, influenza virus, Severe Acute Respiratory Syndrome Virus, *Pseudomonas aeruginosa* and *Mycoplasma pneumoniae* (Kunzelmann et al., 2000, 2006; Hickman-Davis et al., 2006; Chen et al., 2009; Ji et al., 2009). Some of these pathogens have been shown to reduce expression of the ENaC subunit protein (Hickman-Davis et al., 2006; Chen et al., 2009; Ji et al., 2009). We found that PbK infection reduced ENaC activity and expression in the lung, which is likely to contribute to the formation or maintenance of pulmonary oedema by inhibiting fluid re-uptake from the alveolar space. The mechanisms by which pathogens affect ENaC expression and activity are still being elucidated; however, it is probable that the processes are different in a malaria infection compared with the respiratory tract infections. Infectious agents that are transmitted through the respiratory tract can interact directly with the alveolar cell. This direct effect of pathogens on ENaC activity in alveolar cells has been demonstrated in vitro by incubating infectious agents with alveolar epithelial cell lines (Chen et al., 2009; Ji et al., 2009). In contrast, PbK is a blood-borne infection and even when the vessels become congested and leaky, the iRBCs remain in the circulation and do not extravasate into the interstitium or alveoli space. Therefore, the changes in ENaC activity cannot be due to direct interactions of the malaria parasite or iRBC with alveolar cells.

Hypoxia has been shown to lead to reduced ENac activity (Vivona et al., 2001). However, modulation of ENaC activity was not simply due to hypoxia resulting from infection-associated anaemia, as induction of comparable levels of anaemia by administration of PHZ failed to modulate ENaC activity (Fig. 5). Another mechanism for inhibition of ENaC activity is signalling through purinergic receptors. ATP and UTP activate the P2Y2 receptor resulting in phospholipase-C dependent inhibition of ENaC activity (Boncoeur et al., 2010). The cytokines TNF, transforming growth factor (TGF)β and IL1β were shown to decrease expression and activity of ENaC in alveolar epithelial cells (Frank et al., 2003; Dagenais et al., 2004; Roux et al., 2005). However the role of TNF in alveolar fluid clearance (AFC) is complex, as the cytokine was associated with increased amiloride-sensitive AFC in a model of bacterial pneumonia (Rezaiguia et al., 1997). Direct instillation of TNF into the respiratory tract also leads to increased AFC (Fukuda et al., 2001). The effects of TNF on AFC and ENaC activity might depend on the concentration reached, interactions with other cell types and temporal expression. Elevated levels of TNF are found in the circulation during human (Perkins et al., 2000) and rodent (Grau et al., 1987) malaria and are associated with severity of disease. Circulating TGFβ levels are inversely related to severity of disease in human (Perkins et al., 2000) and rodent (Omer and Riley, 1998) malaria. As the iRBCs remain within the circulation, it is likely that soluble molecules, such as cytokines or parasite-secreted factors, are interacting with the alveolar cells to reduce ENaC activity.

Modelling sepsis by injecting mice with LPS results in elevated blood levels of TNF followed by pulmonary oedema (Rojas et al., 2005). As discussed above, PbK-induced lung pathology has similarities to sepsis models. Adding LPS directly to cultured ATII cells causes a decrease in ENaC activity (Boncoeur et al., 2010), but it is not known whether LPS also has indirect effects on ENaC activity. LPS injection, like malaria infection, causes changes in cytokine levels and migration of leukocytes into lung tissue and it is possible that LPS in the bloodstream, or sepsis, could also decrease ENaC activity.

Lung pathology in malaria has been a neglected area in the study of malaria complications. The recent development of three rodent models of malaria-associated lung pathology provides useful tools to study pathogenesis. As they differ in the severity of pathology, comparisons might be useful to investigate the events and factors that determine whether a lung injury progresses to ARDS. The PbK and PbNK65 models use C57BL/6 mice, a genetic background that is common for strains of gene knockout mice, so these models might be useful in identifying molecules involved in pathogenesis. The PbNK65 model provides a severe disease model to look at intervention in malaria-associated ARDS, and dexamethasone has been found to be therapeutic in this system (Van den Steen et al., 2010). PbA infection of DBA/2 mice has revealed that vascular endothelial growth factor (VEGF) levels are associated with development of the severe lung pathology (Epiphanio et al., 2010). The PbK model may be useful for investigating the interactions of anti-malarial drugs with lung pathology. Here, to our knowledge for the first time, we use the model to show that a pathogen in the bloodstream can regulate ENaC activity in the epithelial cell, potentially contributing to pulmonary oedema formation. This suggests that other agents and inflammatory re-

sponses in the circulation, such as sepsis, also have the potential to modulate ENaC activity.

Acknowledgements

This study was supported by a grant from the Australian National Health and Medical Research Council to N.H., H.B. and G.E.G. L.H. received a PhD scholarship from Australian Rotary Health. We thank Meichien Say, Jane Radford and Valery Combes (University of Sydney, Australia) for their assistance with the immunohistochemical analysis.

References

Anstey, N.M., Jacups, S.P., Cain, T., Pearson, T., Ziesing, P.J., Fisher, D.A., Currie, B.J., Marks, P.J., Maguire, G.P., 2002. Pulmonary manifestations of uncomplicated falciparum and vivax malaria: cough, small airways obstruction, impaired gas transfer, and increased pulmonary phagocytic activity. J. Infect. Dis. 185, 1326–1334.

Anstey, N.M., Handojo, T., Pain, M.C., Kenangalem, E., Tjitra, E., Price, R.N., Maguire, G.P., 2007. Lung injury in vivax malaria: pathophysiological evidence for pulmonary vascular sequestration and posttreatment alveolar-capillary inflammation. J. Infect. Dis. 195, 589–596.

Aursudkij, B., Wilairatana, P., Vannaphan, S., Walsh, D.S., Gordeux, V.R., Looareesuwan, S., 1998. Pulmonary edema in cerebral malaria patients in Thailand. Southeast Asian J. Trop. Med. Public Health 29, 541–545.

Belnoue, E., Kayibanda, M., Vigario, A.M., Deschemin, J.C., van Rooijen, N., Viguier, M., Snounou, G., Renia, L., 2002. On the pathogenic role of brain-sequestered alphabeta CD8$^+$ T cells in experimental cerebral malaria. J. Immunol. 169, 6369–6375.

Belperio, J.A., Keane, M.P., Burdick, M.D., Londhe, V., Xue, Y.Y., Li, K., Phillips, R.J., Strieter, R.M., 2002. Critical role for CXCR2 and CXCR2 ligands during the pathogenesis of ventilator-induced lung injury. J. Clin. Invest. 110, 1703–1716.

Boncoeur, E., Tardif, V., Tessier, M.C., Morneau, F., Lavoie, J., Gendreau-Berthiaume, E., Grygorczyk, R., Dagenais, A., Berthiaume, Y., 2010. Modulation of epithelial sodium channel activity by lipopolysaccharide in alveolar type II cells: involvement of purinergic signaling. Am. J. Physiol. Lung Cell Mol. Physiol. 298, L417–L426.

Brooks, M., Kiel, F., Sheehy, T., Barry, K., 1968. Acute pulmonary edema in falciparum malaria. N. Engl. J. Med. 266, 743–749.

Chang, W.L., Jones, S.P., Lefer, D.J., Welbourne, T., Sun, G., Yin, L., Suzuki, H., Huang, J., Granger, D.N., van der Heyde, H.C., 2001. CD8(+)-T-cell depletion ameliorates circulatory shock in *Plasmodium berghei*-infected mice. Infect. Immun. 69, 7341–7348.

Charoenpan, P., Indraprasit, S., Kiatboonsri, S., Suvachittanont, O., Tanomsup, S., 1990. Pulmonary edema in severe falciparum malaria. Hemodynamic study and clinicophysiologic correlation. Chest 97, 1190–1197.

Chen, L., Song, W., Davis, I.C., Shrestha, K., Schwiebert, E., Sullender, W.M., Matalon, S., 2009. Inhibition of Na$^+$ transport in lung epithelial cells by respiratory syncytial virus infection. Am. J. Respir. Cell Mol. Biol. 40, 588–600.

Clark, I.A., Cowden, W.B., 2003. The pathophysiology of falciparum malaria. Pharmacol. Ther. 99, 221–260.

Dagenais, A., Frechette, R., Yamagata, Y., Yamagata, T., Carmel, J.F., Clermont, M.E., Brochiero, E., Masse, C., Berthiaume, Y., 2004. Downregulation of ENaC activity and expression by TNF-alpha in alveolar epithelial cells. Am. J. Physiol. Lung Cell Mol. Physiol. 286, L301–L311.

de Souza, J.B., Hafalla, J.C., Riley, E.M., Couper, K.N., 2010. Cerebral malaria: why experimental murine models are required to understand the pathogenesis of disease. Parasitology 137, 755–772.

Elias, N., Rafii, B., Rahman, M., Otulakowski, G., Cutz, E., O'Brodovich, H., 2007. The role of alpha-, beta-, and gamma-ENaC subunits in distal lung epithelial fluid absorption induced by pulmonary edema fluid. Am. J. Physiol. Lung Cell Mol. Physiol. 293, L537–L545.

Epiphanio, S., Campos, M.G., Pamplona, A., Carapau, D., Pena, A.C., Ataide, R., Monteiro, C.A., Felix, N., Costa-Silva, A., Marinho, C.R., Dias, S., Mota, M.M., 2010. VEGF promotes malaria-associated acute lung injury in mice. PLoS Pathog. 6, e1000916.

Frank, J., Roux, J., Kawakatsu, H., Su, G., Dagenais, A., Berthiaume, Y., Howard, M., Canessa, C.M., Fang, X., Sheppard, D., Matthay, M.A., Pittet, J.F., 2003. Transforming growth factor-beta1 decreases expression of the epithelial sodium channel alphaENaC and alveolar epithelial vectorial sodium and fluid transport via an ERK1/2-dependent mechanism. J. Biol. Chem. 278, 43939–43950.

Fukuda, N., Jayr, C., Lazrak, A., Wang, Y., Lucas, R., Matalon, S., Matthay, M.A., 2001. Mechanisms of TNF-alpha stimulation of amiloride-sensitive sodium transport across alveolar epithelium. Am. J. Physiol. Lung Cell Mol. Physiol. 280, L1258–L1265.

Grau, G.E., Fajardo, L.F., Piguet, P.F., Allet, B., Lambert, P.H., Vassalli, P., 1987. Tumor necrosis factor (cachectin) as an essential mediator in murine cerebral malaria. Science 237, 1210–1212.

Hickman-Davis, J.M., McNicholas-Bevensee, C., Davis, I.C., Ma, H.P., Davis, G.C., Bosworth, C.A., Matalon, S., 2006. Reactive species mediate inhibition of alveolar type II sodium transport during mycoplasma infection. Am. J. Respir. Crit. Care Med. 173, 334–344.

Ji, H.L., Song, W., Gao, Z., Su, X.F., Nie, H.G., Jiang, Y., Peng, J.B., He, Y.X., Liao, Y., Zhou, Y.J., Tousson, A., Matalon, S., 2009. SARS-CoV proteins decrease levels and activity of human ENaC via activation of distinct PKC isoforms. Am. J. Physiol. Lung Cell Mol. Physiol. 296, L372–L383.

Kunzelmann, K., Beesley, A.H., King, N.J., Karupiah, G., Young, J.A., Cook, D.I., 2000. Influenza virus inhibits amiloride-sensitive Na$^+$ channels in respiratory epithelia. Proc. Natl. Acad. Sci. USA 97, 10282–10287.

Kunzelmann, K., Scheidt, K., Scharf, B., Ousingsawat, J., Schreiber, R., Wainwright, B., McMorran, B., 2006. Flagellin of *Pseudomonas aeruginosa* inhibits Na$^+$ transport in airway epithelia. FASEB J. 20, 545–546.

Li, T., Folkesson, H.G., 2006. RNA interference for alpha-ENaC inhibits rat lung fluid absorption in vivo. Am. J. Physiol. Lung Cell Mol. Physiol. 290, L649–L660.

Li, T., Koshy, S., Folkesson, H.G., 2007. Involvement of {alpha}ENaC and Nedd4-2 in the conversion from lung fluid secretion to fluid absorption at birth in the rat as assayed by RNA interference analysis. Am. J. Physiol. Lung Cell Mol. Physiol. 293, L1069–L1078.

Lichtman, A.R., Mohrcken, S., Engelbrecht, M., Bigalke, M., 1990. Pathophysiology of severe forms of falciparum malaria. Crit. Care Med. 18, 666–668.

Lovegrove, F.E., Gharib, S.A., Pena-Castillo, L., Patel, S.N., Ruzinski, J.T., Hughes, T.R., Liles, W.C., Kain, K.C., 2008. Parasite burden and CD36-mediated sequestration are determinants of acute lung injury in an experimental malaria model. PLoS Pathog. 4, e1000068.

Matalon, S., Bridges, R.J., Benos, D.J., 1991. Amiloride-inhibitable Na$^+$ conductive pathways in alveolar type II pneumocytes. Am. J. Physiol. 260, L90–L96.

Menezes, S.L., Bozza, P.T., Neto, H.C., Laranjeira, A.P., Negri, E.M., Capelozzi, V.L., Zin, W.A., Rocco, P.R., 2005. Pulmonary and extrapulmonary acute lung injury: inflammatory and ultrastructural analyses. J. Appl. Physiol. 98, 1777–1783.

Mitchell, A.J., Hansen, A.M., Hee, L., Ball, H.J., Potter, S.M., Walker, J.C., Hunt, N.H., 2005. Early cytokine production is associated with protection from murine cerebral malaria. Infect. Immun. 73, 5645–5653.

Mitchell, A.J., Pradel, L.C., Chasson, L., Van Rooijen, N., Grau, G.E., Hunt, N.H., Chimini, G., 2010. Technical advance: autofluorescence as a tool for myeloid cell analysis. J. Leukoc. Biol. 88, 597–603.

Omer, F.M., Riley, E.M., 1998. Transforming growth factor beta production is inversely correlated with severity of murine malaria infection. J. Exp. Med. 188, 39–48.

Perfetto, S.P., Chattopadhyay, P.K., Roederer, M., 2004. Seventeen-colour flow cytometry: unravelling the immune system. Nat. Rev. Immunol. 4, 648–655.

Perkins, D.J., Weinberg, J.B., Kremsner, P.G., 2000. Reduced interleukin-12 and transforming growth factor-beta1 in severe childhood malaria: relationship of cytokine balance with disease severity. J. Infect. Dis. 182, 988–992.

Planes, C., Blot-Chabaud, M., Matthay, M.A., Couette, S., Uchida, T., Clerici, C., 2002. Hypoxia and beta 2-agonists regulate cell surface expression of the epithelial sodium channel in native alveolar epithelial cells. J. Biol. Chem. 277, 47318–47324.

Potter, S., Chan-Ling, T., Ball, H.J., Mansour, H., Mitchell, A., Maluish, L., Hunt, N.H., 2006. Perforin mediated apoptosis of cerebral microvascular endothelial cells during experimental cerebral malaria. Int. J. Parasitol. 36, 485–496.

Rezaiguia, S., Garat, C., Delclaux, C., Meignan, M., Fleury, J., Legrand, P., Matthay, M.A., Jayr, C., 1997. Acute bacterial pneumonia in rats increases alveolar epithelial fluid clearance by a tumor necrosis factor-alpha-dependent mechanism. J. Clin. Invest. 99, 325–335.

Rojas, M., Woods, C.R., Mora, A.L., Xu, J., Brigham, K.L., 2005. Endotoxin-induced lung injury in mice: structural, functional, and biochemical responses. Am. J. Physiol. Lung Cell Mol. Physiol. 288, L333–L341.

Roux, J., Kawakatsu, H., Gartland, B., Pespeni, M., Sheppard, D., Matthay, M.A., Canessa, C.M., Pittet, J.F., 2005. Interleukin-1beta decreases expression of the epithelial sodium channel alpha-subunit in alveolar epithelial cells via a p38 MAPK-dependent signaling pathway. J. Biol. Chem. 280, 18579–18589.

Schofield, L., Hewitt, M.C., Evans, K., Siomos, M.A., Seeberger, P.H., 2002. Synthetic GPI as a candidate anti-toxic vaccine in a model of malaria. Nature 418, 785–789.

Senaldi, G., Vesin, C., Chang, R., Grau, G.E., Piguet, P.F., 1994. Role of polymorphonuclear neutrophil leukocytes and their integrin CD11a (LFA-1) in the pathogenesis of severe murine malaria. Infect. Immun. 62, 1144–1149.

Tan, L.K., Yacoub, S., Scott, S., Bhagani, S., Jacobs, M., 2008. Acute lung injury and other serious complications of *Plasmodium vivax* malaria. Lancet Infect. Dis. 8, 449–454.

Van den Steen, P.E., Geurts, N., Deroost, K., Van Aelst, I., Verhenne, S., Heremans, H., Van Damme, J., Opdenakker, G., 2010. Immunopathology and dexamethasone therapy in a new model for malaria-associated acute respiratory distress syndrome. Am. J. Respir. Crit. Care Med. 181, 957–968.

Vermaelen, K., Pauwels, R., 2004. Accurate and simple discrimination of mouse pulmonary dendritic cell and macrophage populations by flow cytometry: methodology and new insights. Cytometry A 61, 170–177.

Vivona, M.L., Matthay, M., Chabaud, M.B., Friedlander, G., Clerici, C., 2001. Hypoxia reduces alveolar epithelial sodium and fluid transport in rats: reversal by beta-adrenergic agonist treatment. Am. J. Respir. Cell Mol. Biol. 25, 554–561.